EXTERNAL TRANSMITTAL AUTHORIZED
ORNL
Central Files Number
60-5-109

66

AN INVESTIGATION OF THE STRUCTURAL INTEGRITY OF SELECTED COMPONENTS OF THE OAK RIDGE RESEARCH REACTOR

J. M. Corum
B. L. Greenstreet
R. L. Maxwell
M. W. Rosenthal

OAK RIDGE NATIONAL LABORATORY
operated by
UNION CARBIDE CORPORATION
for the
U.S. ATOMIC ENERGY COMMISSION

DISCLAIMER

External Transmittal Authorized
ORNL
Central Files Number
60-5-109

AN INVESTIGATION OF THE STRUCTURAL INTEGRITY OF SELECTED COMPONENTS OF THE OAK RIDGE RESEARCH REACTOR

J. M. Corum
B. L. Greenstreet
R. L. Maxwell
M. W. Rosenthal

DATE ISSUED
JUL 22 1960

OAK RIDGE NATIONAL LABORATORY
Oak Ridge, Tennessee
operated by
UNION CARBIDE CORPORATION
for the
U. S. ATOMIC ENERGY COMMISSION

CONTENTS

ABSTRACT

An investigation was made to determine the structural behavior of selected components of the Oak Ridge Research Reactor for increased power level conditions. It was found that a reactor cooling water outlet temperature of 150°F will cause severe plastic strain cycling in the aluminum housings for the large test facilities. Increasing the reactor cooling water flow rate of 22 000 gpm will cause plastic deformations in certain regions of the core box. These latter deformations can be tolerated, but the full implications associated with any change in pressure differential must be understood before adopting the above flow rate.

SUMMARY

Critical regions of the Oak Ridge Research Reactor system were studied to determine the feasibility of increasing the reactor cooling water outlet temperature and the feasibility of increasing the flow rate. It was found that portions of the aluminum housings for the large test facilities undergo plastic strain cycling at the present operating conditions (outlet water temperature of 132°F and a flow rate of 16 000 gpm), and increasing the coolant outlet temperature to 150°F would probably lead to cracking after a relatively small number of cycles from zero to full power. The beam hole tubes are also subjected to strain cycling, but the magnitudes of the alternating plastic strains are less than in the case of the housings for the large test facilities.

The combined pressure and thermal stresses in the walls of the core box will probably exceed the yield strength of the material for a cooling water flow rate of 22 000 gpm. Hence, yielding and redistribution of the stresses will occur, and, although measurable deformations of the flat plates are likely, the structural integrity of the core box will be maintained. Very little, if any, yielding occurs at a 16 000 gpm flow rate.

It should be recognized that the pressure loading associated with the 22 000 gpm flow rate is nearly equivalent to the hydrostatic test pressure for this compartment. The ASME Code gives 2/3 of the test pressures as the maximum working pressure. Although this limit was set on the basis of a large background of experience, it may be exceeded provided deformations and the associated stress redistributions can be tolerated. However, because poor welds or other defects may be present, there is no way to predict the precise load-carrying ability of any compartment. Hence, the pressure in any section should never exceed the hydrostatic test pressure.

The magnitudes of the plastic strains in the housings for the large test facilities and the strain cycling characteristics of the materials were established on the basis of the scant data available. Since it appears that portions of the structure are being strain cycled under the present operating conditions, the importance of a program to assess the structural behavior more accurately cannot be overemphasized. It is recommended that additional strain measurements be made on the highly strained regions of the dished head, that stress versus strain curves be obtained from tensile tests using materials corresponding to those of the reactor, and that a test program be initiated for producing applicable plastic strain cycling data. With these data, better predictions can be made regarding the effects of the present operating conditions.

INTRODUCTION

If the power level of the Oak Ridge Research Reactor is raised, the effectiveness of the machine will be greatly enhanced. In order to increase the heat removal capability of the present heat exchangers, it has been proposed that the reactor coolant outlet temperature be increased from 132° to 150°F. Consideration is also being given to raising the coolant flow rate from 16 000 to 22 000 gpm to permit an increase in core power to 45 Mw following the installation of additional heat exchange equipment. An increase in flow rate would be accompanied by higher hydrostatic pressures in the reactor core; a higher water temperature would result in greater thermal expansion stresses throughout the system.

The elements examined are those that would be affected most by the proposed changes in operating conditions. These are the cooling water return lines, the pool-interconnection lines which are attached to the return lines and lie within the biological shield, the large test facilities, the beam hole tubes, the pool side facility flat plate, and the regions of the core box that are encompassed by the obrounds of the large facilities. In each case the calculated stresses for designated temperatures and pressures are given. These are then interpreted in terms of materials behavior and the structural integrity of the unit. The appendix describes the mechanical properties of the materials, and a table of the allowable stresses, as given by the ASME Unfired Pressure Vessel Code, is included.

The analysis of the large facilities presented a very complex problem for which the accuracy of the theoretical model could not be determined without comparing the results with experimental data. Because of this, strain measurements were made on the actual reactor components, and, finally, a 1/4-scale model of that portion of the obround which

is outside the pressure vessel (see Fig. 1) was tested.

The strain measurements were made with the help and direction of staff members from the Mechanical Engineering Department of the University of Tennessee, and the scale model was constructed and tested by this group. The authors wish to thank Professor R. W. Holland, Mr. C. Fisher, Mr. M. Milligan, and Mr. C. Wilson for their cooperation and participation in this work.

DESCRIPTION OF EACH ANALYSIS

The following brief description of each analysis includes the data pertinent to the investigations, the conditions taken, a summary of the work done, and an interpretation of the results obtained therefrom.

Piping Analysis

From a preliminary examination it appeared that, in the event of an increase in reactor operating temperature, large thermal expansion stresses would be developed in at least three piping lines. These lines were isolated and examined by the method outlined in Kellogg's Expansion Stresses and Reactions in Piping Systems.[1] [1] A summary of these analyses follows.

Cooling Water Return Line 101 and 102

Referring to Fig. 2, the two 18 in. lines were taken to be anchored at a point inside the pool structure as shown, and the 24 in. line was taken to be anchored at the location of the 45° bend outside the reactor building. The isolated line is shown in Fig. 3. In this and all subsequent pipe calculations, the 90° bends were assumed to be square in order to simplify calculations. The pipe material is 5154 aluminum. The following material constants were used:

Coefficient of thermal expansion, α	13×10^{-6} in./in.-$^{\circ}$F
Modulus of elasticity, E	10×10^{6} psi
Poisson's ratio, μ	0.3

[1] Numbers in brackets refer to similarly numbered references at the end of this report.

Referring to Fig. 3 the pipe sizes and properties are given in Table I.

Table I. Properties of Piping Used for ORR Cooling Water Lines

Line	Outside Diameter (in.)	Wall Thickness (in.)	Section Modulus ($in.^4$)
O-D	24	0.313	1630
D-A	18	0.250	550
D-B	18	0.250	550

In the analysis, an internal gage pressure of 75 psig was considered. The twelve simultaneous equations, which were obtained by the method outlined in Kellogg's book, were solved on the IBM 704. The torsional and bending moments at each point were then calculated. These moments are shown in Figs. 4, 5, and 6 for the X, Y, and Z planes respectively, where the X, Y, and Z planes are any planes perpendicular to the similarly designated coordinate axes. Bending moments which produce compression in the positive fibers are shown as positive. In these figures the positive side of a line is that corresponding to the positive direction of the appropriate coordinate axis. Torsional moments which act counterclockwise on the end of a line nearest the origin when one is looking along the line in the direction leading to the origin are shown as positive.

The maximum combined stresses occur at point A-4. Consider a small rectangular element cut from the surface of the pipe and perpendicular to the plane of the maximum bending moment. The element is acted upon by a bending stress, σ_B, a hoop stress, σ_θ, and a shear stress, τ, which is due to the torsional moment. Since the bending and torsional stresses are linear with temperature, the values of these stresses at point A-4 may be expressed as a function of the temperature

change. Thus

$$\sigma_B = 82.56\,\Delta T, \qquad \tau = 2.73\,\Delta T \quad .$$

For an internal pressure of 75 psig, the tangential stress, σ_θ, is 2625 psi. The maximum principle stresses and maximum shearing stress for a cooling water exit temperature of 150°F are given in Table II, which summarizes the piping stresses.

Cooling Water Return Line from Pump House to Anchor at Cooler

The section of line considered is shown isolated in Fig. 7. The fixed points represent anchors at the pump house and between the fourth and fifth branch risers at the cooler. It was assumed that the Victaulic-type pipe couplings installed in each branch riser limit the reactions of these lines on the 24 in. header to negligible values. As in the previous line, the pipe material is 5154 aluminum so that the material properties are the same as those previously tabulated. The pipe size is 24 in. o.d. with the same properties as those given for line O-D in Table I. The bends were assumed to be angular.

The internal gage pressure was taken to be 75 psig. Solution of three simultaneous equations and calculation of the moments at each point gave the moment distribution shown in Fig. 8. The maximum stress occurs in the 45°, 9/16 in. wall, long radius elbow at B. In the bending of a curved tube by moments in the plane of the bend, flattening of the cross section during bending changes the maximum stress as predicted by elementary theory by a factor β, which depends on the proportions of the bend. For the elbow at B, β is approximately three. When this value is used the maximum bending stress as a function of temperature change becomes

$$\sigma_1 = 85.8\,\Delta T \quad .$$

The hoop stress for a 75 psig internal pressure is 2800 psi. The maximum principle stresses and maximum shearing stress for a cooling water exit temperature of 150°F are given in Table II.

Lines 138 and 138 – Pool-Interconnection Lines

Referring to Fig. 2, one end of each pool-interconnection line is attached to the lines 101 or 102. The other end is welded to the aluminum pool liner just inside the pool. The section of line between these points is shown isolated in Fig. 9. Reactor piping drawings call for an anchor located between points B and C. However, an examination of photographs taken during construction indicates that no anchor was used. The pipe material is 6063-T6 aluminum with the following material constants:

Coefficient of thermal expansion	13.0×10^{-6} in./in.-°F
Modulus of elasticity	10.0×10^{6} psi
Poisson's ratio	0.3

The pipe has a 3 in. o.d., a 0.216 in. wall thickness, and a section modulus of 3.017 $in.^4$

In the analysis, expansion of the cooling water return line was taken into account, and the same temperature change was considered for both lines. The internal gage pressure was taken to be zero. After solution of the six simultaneous equations, the torsional and bending moments at each point were calculated. The results of these calculations are shown in Figs. 10, 11, and 12.

The maximum combined stresses occur at point C-4. A rectangular element cut from the surface as before will be acted upon by a bending stress, σ_B, and a shear stress, τ. These stresses as a function of temperature change are

$$\sigma_B = 20.9\,\Delta T, \quad \tau = 2.99\,\Delta T \quad .$$

The maximum principle stresses and maximum shearing stress for a cooling water exit temperature of 150°F are given in Table II.

Summary of Maximum Principle Stresses and Maximum Shearing Stresses in Pipe Lines

Considering a cooling water exit temperature of 150°F and an installation temperature of 75°F (neglecting cold springing), ΔT is equal to 75°F. Table II gives the maximum principle stresses in the three lines under consideration. An internal pressure of 75 psig was considered in the cooling water return lines, and an internal gage pressure of zero was considered in the pool-interconnection lines.

Table II. Maximum Principle Stresses and Maximum Shearing Stresses in Pipe Lines for ΔT = 75°F

Line	Maximum Principle Stresses σ_1(psi)	σ_2(psi)	Maximum Shearing Stress (psi)
Cooling Water Return Lines 101 and 102[a]	6200	2610	1800
Cooling Water Return From Pump House to Anchor at Cooler[a]	6450	2800	1830
Pool-Interconnection Lines 137 and 138[b]	1600	-31	814

[a]An internal pressure of 75 psig was considered.

[b]An internal gage pressure of zero was considered.

A comparison of the stresses in Table II with the values in Table A.II of the appendix shows that these stresses are below those allowed by the ASME Code. Thus, the lines can be considered safe for

an operating temperature of 150°F and an internal pressure of 75 psig.

Analysis of Large Facilities

Thermal expansion of the reactor tank in the vertical and radial directions induces stresses of an appreciable magnitude in the obround and dished head. The loads and moments acting on the obround were obtained by theoretical considerations; from these the maximum stresses in the obround and dished head were predicted. Due to several uncertainties in the theoretical analysis, a limited number of strain measurements were made on the actual reactor facilities. In addition, a 1/4-scale model of the large facilities was constructed and tested at the University of Tennessee. A brief description of each of the above mentioned analyses and the results obtained therefrom follows.

Theoretical Analysis

The theoretical analysis was based on the obround behaving as a beam loaded with forces and moments at the three points corresponding to the attachments to the obround, of the dished head, tank wall, and core box as shown in Fig. 13. It was assumed that the obround was completely restrained from rotation at the tank wall and at the core box connection. The rotation of the dished head due to the moment exerted on it by the obround was included in the analysis. The behavior of the dished head, tank wall, and core box with regard to in-plane deformations and their associated stress distributions was assumed to be that of a flat plate loaded with a concentrated force in the plane of the plate. By taking into account the in-plane deflections of the dished head, tank wall, and core box due to the force exerted on each element by the obround, it was possible to write two equations relating the deflections of the obround to the vertical thermal expansion of

the tank unit at the obround centerline. In these equations both the shear and bending deflections of the obround were considered.

Immediately prior to welding the large facilities to the tank unit, the temperature of the tank was raised to 105°F. In order to account for uncertainties in measuring the true tank temperature, the temperature deviation from 100°F was considered in determining the thermally induced stresses. An operating temperature of 150°F causes a vertical reaction of 766 000 lb at the obround-dished head junction. At the tank wall and core box, the reactions were 585 000 lb and 181 000 lb, respectively. The moment exerted on the obround by the dished head was calculated to be 12 250 in.-lb, and the moment exerted by the tank wall was 6 300 000 in.-lb.

The maximum stresses occur in the dished head and obround near the intersection of the two. The total stress in the dished head is due to the vertical reaction of the obround, the moment exerted on the dished head by the obround, and a horizontal force due to radial expansion of the reactor tank. Using these conditions the maximum principle stress in the dished head was calculated to be

$$\sigma_1 = -16\,900 \text{ psi} \quad .$$

The maximum calculated bending stress in the obround was

$$\sigma = 7\,200 \text{ psi} \quad ,$$

and the transverse shearing stress in this member was found to be

$$\tau_{max} = 10\,300 \text{ psi} \quad .$$

Strain Measurements on the Large Facilities

Mechanical strain-measuring instruments (Huggenberger tensometers) were attached to the large facilities at various positions as shown in Fig. 14. Due to the limited space between the dished head and tank

wall, the maximum principle stress in the dished head could not be measured directly. The instruments were positioned in the pool by the use of long pieces of aluminum tubing. The following procedure was used to obtain measurements: The reactor coolant temperature was raised to approximately 105°F by reactor power. The reactor was then shut down, the water level was lowered to the reactor tank top, and the instruments were positioned. Then by use of the air coolers, the temperature was lowered approximately 30°F in steps of 10°F each. Using binoculars, the tensometer readings were made at the end of each incremental temperature drop.

Table III gives the measured strains at each position for the indicated measured temperature drop. Using the elastic stress-strain

Table III. Results of ORR Strain Measurements

Position	Strain (in./in.)	Temperature Drop (°F)
1	0.00040	27
2	-0.00006	27
3	0.00024	27
4	-0.00005	28

relations for isotropic materials stressed below the proportional limit along with the empirical relations regarding stress states in the dished head, the stresses at each of the above four points were found. Table IV gives the results of these calculations along with values, for the same temperature drops, predicted by the theoretical analysis.

Strain Gage Analysis of Large Facility Model

Table IV shows that considerable discrepancy existed between the analytical and experimental results. Because of this a 1/4-scale

Table IV. Maximum Stresses Obtained From Strain Measurements

Position	Stress From Strain Measurements (psi)	Theoretically Predicted Stress (psi)
1	τ = 3030	τ = 5580
2	σ = - 580	σ = -1810
3	σ = 2290	σ = 2470
4	τ = 449	τ = 886

aluminum model of the large facilities was constructed at the University of Tennessee for the purpose of performing electrical resistance strain gage analyses on the model under various loadings. A sketch of the model showing the method of loading is shown in Fig. 15. A total of 46 strain gages were located at various positions on the model. A photograph of the model during testing is shown in Fig. 16.

Although several separate combinations of loadings were used, only the results of the one which most nearly fits the given conditions will be presented here. For ease of comparison the loadings used on the model have been converted to loadings which, when applied to the full-scale large facilities, will produce stresses equal to those obtained in the model. Keeping this in mind, the stresses at seven key points are given in Table V for the case where the force, P, was equal to 32 000 lb and the moment, aF, was chosen so that the resultant moment at point O (see Fig. 15) was zero. The seven gage positions are shown in Fig. 17. It should be noted that the above loading combination is that which would actually occur in the full-scale facilities only if the dished head and tank completely restrain the ends of the obround against rotation.

Table V. Stresses Obtained From Model Analysis
($P = 32\,000$ lb, $M_{\text{about } O} = 0$)

Point	Type of Stress	Stress (psi)
1	Normal	-4810
2	Normal	-3200
3	Normal	- 526
4	Normal	-1390
5	Normal	1550
6	Normal	100
7	Shear	564

Interpretation of Results

An attempt will be made to interpret the data which have been presented in terms of the effects of cyclic loadings on the large facility components. It should be understood that the stresses resulting from thermal expansion were obtained on the basis of the material following Hooke's Law. Actually, many of the stresses are above the proportional limit of the material. Thus, these stress values are never reached because the expansion is absorbed in plastic strain.

Due to normal reactor startup and shutdown, the thermal expansions of the components are cyclic in nature. Thus, the yielding of the material at various localized points is also cyclic in nature, and the problem becomes one of fatigue due to plastic strain reversals. That is, for a given plastic strain range, there is a limiting number of cycles which the material may be subjected to before failure occurs.

Correlations of plastic strain versus number of cycles are obtained in much the same way as ordinary fatigue curves are obtained. L. F. Coffin [2][3][4] has found that plots of plastic-strain range versus cycles to failure on logarithmic coordinates are best fitted by straight lines

with a slope equal to -1/2. These observations do not depend upon the material that is being tested, the temperature of testing, nor the manner in which the fatigue test is made. Furthermore, Coffin has found that if the fracture strain value is placed on the log-log plot at N = 1/4, a straight line through this point with a slope of -1/2 gives a good approximation to the true curve.

In the absence of experimental cyclic-strain data, the curves for 1100-0, 5052-0, and 5154-0 aluminum alloys were constructed as described above; these are shown in Fig. 18. It should be noted that if the ductility of the materials is lower than that corresponding to an -0 temper, the curves will be displaced downward.

From the results of the theoretical analysis on the large facilities, a maximum stress of -16 900 psi in the region of the dished head immediately above the obround is predicted. By comparing the results of the strain analysis on the actual reactor facilities with the same stresses as predicted by the theoretical model, it is seen that the theoretical values are somewhat high. However, due to space limitations the strains in the immediate vicinity of the obround could not be measured with the tensometers used. Referring to Table V, which gives the results of the model analysis, it is seen that the stresses in the region of the dished head near the obround (points 1 and 2) are much larger, with respect to the transverse shearing stress in the obround, than would be predicted. This same result was observed in all of the model tests regardless of the combination of loadings. In all cases the maximum stress in the dished head was at least eight times greater than the transverse shearing stress in the obround. The transverse shearing stresses are very nearly the same as would be predicted by dividing the transverse force by the cross-sectional area of the obround.

Assuming that the shearing stress in the obround for a temperature change of 27°F is that obtained by actual measurement, the transverse shearing stress for a temperature change of 50°F would be

$$\tau = 5610 \text{ psi} \quad .$$

Provided the maximum principle stress in the dished head is at least eight times this value, one obtains

$$\sigma_{max} = 44\ 880 \text{ psi} \quad .$$

This stress is much above the yield point of the material so that in actuality it will never be reached because most of the tank expansion will be absorbed in plastic strain.

The stress in the dished head decreases rapidly with distance from the obround, and any plastic deformation of the material is localized. In order to estimate the plastic strain, a plot of "elastic" stress versus distance from the top of the obround was made. It was then assumed that the depth of the plastic region is determined by the distance to the point where the curve crosses the yield stress line. This method gave a 2 in. depth, and it was further assumed that the vertical movement was absorbed by uniform strain in the region thus defined. The method does not give a conservative estimate of the maximum strain, but it provides a means for gaining an insight into the structural behavior of the element.

Proceeding on the basis of the model described, a 50°F increase in temperature above 100°F produces a plastic strain of 0.011 in./in. From Fig. 18 for 5154-0, the number of cycles to failure is 460. In practice, the number of cycles obtained from the curves should be reduced by a factor of ~10 to allow for uncertainties in materials properties, since the test data usually represent that collected in carefully controlled experiments. Thus, the dished head could fail after only 46 cycles. This, of course, assumes that the facilities have had no previous strain cycling. Actually the facilities are being strain cycled under the present operating conditions.

The above assumption that all of the vertical movement is absorbed by plastic strain of the dished head is not true because of elastic

deformations at other points. On the other hand, the localized yielding might very well occur over a region much shorter than two inches. In any event, in the absence of more conclusive information, it may be concluded that the dished head would very definitely undergo severe localized strain cycling and that there exists some relatively small number of cycles above which failure of the facilities would occur.

It cannot be overemphasized that the magnitude of the plastic strains in the large facilities and the strain cycling characteristics of the materials were established on the basis of the scant data available. Since it appears that portions of the dished head are being strain cycled even under the present operating temperatures, the problem should definitely be pursued further.

Thus, it is recommended that two specific steps be taken to obtain the information necessary to more accurately assess the structural integrity of the large facilities under the present operating temperatures. First, additional strain measurements should be made on the large facilities. These measurements should be made while going from room temperature to the temperature corresponding to full power, and special tensometers which allow measurements to be made on the dished head in the region immediately above the obround should be used. In this manner, a better estimate of the actual plastic strains which occur would be obtained. As a second step, stress versus strain curves should be obtained from tensile tests using materials corresponding to those of the reactor, and a test program should be initiated for producing applicable plastic strain cycling data. Having these data and an estimate of the plastic strains which actually occur, better predictions can be made regarding the effects of the present operating conditions.

Analysis of Beam Hole Tubes

Vertical and radial thermal expansion of the reactor tank will induce bending and compressive stresses in each of the six beam hole

tubes (see Fig. 1). The deflection of the beam hole tubes due to vertical tank expansion will be greatest for those tubes which are highest from the pool floor. In addition, the shorter tubes will have the greatest bending and compressive stresses. From these considerations, beam hole tube BH-6 was chosen for examination. A sketch of BH-6 with the dimensions used in the analysis is shown in Fig. 19. The material of the beam hole tubes is 1100 aluminum.

The analysis was based on the beam hole tubes behaving as a beam with transverse and axial loading. For the forces involved, the deflections of the tank wall and core box are negligible; therefore, the section of the tubes between the tank wall and core box was neglected. The ends were assumed to be rigidly fixed against rotation by the tank wall and the concrete pool wall. In order to consider the effects of the varying cross section of the tubes, the moment distribution was found by use of the area-moment methods.

Considering a reactor operating temperature of 150°F, the maximum stress was found to occur at section A-A (see Fig. 19). If an elastic system is assumed to exist, the maximum bending stress at section A-A is found to be 3560 psi, and the compressive stress due to radial tank expansion is 8040 psi. Thus, the maximum total stress is

$$\sigma_{max} = -\ 12\ 600 \text{ psi} \quad .$$

Referring to Table A.I in the appendix, the maximum stress is above the yield point of the material. Thus, this stress will never be reached and the tube will undergo plastic strain cycling. Considering the radial tank expansion only, and referring to Fig. 19, the length of tube with the small cross section A-A will yield before the sections with larger cross sections. Assuming for the material a stress-strain diagram with no strain hardening beyond the yield point, the stress at the larger cross sections will never become greater than that corresponding to the yield point stress in the small section. Thus, any additional deflection occurring after the yield point stress is reached

in the small section will be absorbed by plastic strain of the small section. For an operating tank temperature of 150°F, the natural plastic strain will be 0.0026 in./in. From Fig. 18, failure might occur after 3000 cycles. The bending effects due to vertical tank expansion will increase the plastic strain so that the number of cycles to failure will be decreased somewhat.

Analysis of Tank Components

Examination of the various tank components indicated that an investigation of the stresses in the pool side facility flat plate and the portion of the core box sides encompassed by the obround was warranted. The components were examined for both thermal stresses and stresses due to pressure differences across the plates. A reactor coolant flow of 16 000 and 22 000 gpm was considered in each case. The material of both plates is the aluminum alloy 5052. A summary of these analyses follows.

Stress Analysis

The pool side facility flat plate is shown in Fig. 13. Calculations were made assuming both a normal pool level and a pool level at the reactor tank top. For these conditions coolant flow rates of 16 000 gpm and 22 000 gpm were investigated. For a normal pool level and a flow rate of 16 000 gpm, the pressure differential across the flat plate varies linearly from 6.8 psi at the bottom edge to 22.7 psi at the top edge. For a coolant flow rate of 22 000 gpm, the corresponding values are 12.0 and 40.1 psi respectively. If the pool level is at the reactor tank top, the above values are increased by 4.6 psi. The temperature distribution, through the thickness of the plate due to gamma heating, was taken to be

$$T = 50 - \frac{40}{C^2} y^2 + \frac{10}{C} y$$

where y is measured from the center of the plate. The positive direction for y is in the direction of the core, and one-half of the plate thickness is denoted by C. This distribution is believed to be conservative, with regard to thermal stresses, even for a power level of 45 Mw.

The maximum stresses occur when it is assumed that the edges of the plate are completely fixed. If the stress concentration factors due to the presence of the cooling holes are neglected, the maximum stress in the plate occurs at the midpoint of the upper edge, and is due to moments in the vertical plane which is perpendicular to the plane of the plate. For a low pool level and a coolant flow rate of 22 000 gpm, the stress distributions through the plate at the above point are shown in Fig. 20. The maximum combined stress is 14 000 psi while the maximum stress due to pressure is 9300 psi.

It was estimated that the presence of the cooling holes would introduce a stress concentration factor of approximately three in the region near the holes. This factor applies only to stresses due to moments in the horizontal plane. Since the cooling holes were not considered in the temperature distribution, the stress concentration factor was not applied to the thermal stress. Using these conditions, the maximum stresses now occur on the sides of the plate at points just above the horizontal centerline. These stresses are due to moments acting in the horizontal plane, and they reach their maximum value in the localized region of the holes. The maximum stress and the thermal stress component for each condition are given in Table VI.

The portions of the core box encompassed by the obrounds of the large facilities as shown in Fig. 13 were also considered. It was assumed in this analysis that the space inside the obround was at atmospheric pressure. For this condition and a coolant flow rate of 22 000 gpm, the pressure differential varies linearly from 25.5 psi at the

Table VI. Maximum Localized Stress in Pool Side Facility Flat Plate

Conditions	Maximum Stress (psi)	Pressure Stress Component (psi)	Thermal Stress Component (psi)
High Pool Level:			
22 000 gpm	-23 190	17 750	5440
16 000 gpm	-15 490	10 050	5440
Low Pool Level:			
22 000 gpm	-26 190	20 750	5440
16 000 gpm	-18 490	13 050	5440

lower point to 47.5 psi at the upper point. The corresponding values for a coolant flow rate of 16 000 gpm are 19.1 and 31.0 psi respectively. The temperature distribution through the thickness of the plate was taken to be

$$T = 4.4 + \frac{4.4}{C^2} y^2 + \frac{8.8}{C} y$$

with y again measured from the center of the plate in the direction of the core box and C denoting one-half of the total thickness.

In the analysis the portion of the plate to be examined was taken to be elliptical in shape. The maximum stresses occur when it is assumed that the edges of the plate are completely fixed. If the stress concentration factors due to the presence of the cooling holes are neglected, the maximum total stress (thermal and pressure stress) occurs on the vertical centerline of the plate slightly above the horizontal centerline. The magnitude of this stress, for a coolant flow rate of 22 000 gpm, is

$$\sigma_{max} = -6540 \text{ psi} \quad .$$

The maximum pressure stress is ± 5040 psi, and the maximum thermal stress is -3540 psi.

As in the analysis of the previous plate, it was estimated that the presence of the cooling holes would introduce a stress concentration factor of approximately three near the holes. Again, this factor applies only to stresses due to moments in the horizontal plane. The temperature distribution was calculated disregarding the effect of the cooling holes; therefore, the stress concentration factor was not applied to the thermal stress. Using these conditions the maximum total stress occurs in the localized region near the holes, and for a coolant flow rate of 22 000 gpm, it is

$$\sigma_{max} = - 10\ 900 \text{ psi} \quad .$$

Interpretation of Results

Neglecting the presence of the cooling holes and referring to Fig. 20, it is seen that although the total calculated "elastic" stress in the pool side facility flat plate is above the yield point stress of the material, it is below the endurance limit. Plastic deformation will occur, but since this is a flat plate, large deformations will give rise to tensile membrane stresses and the compressive bending stresses due to the pressure differential will be reduced. Considering the localized stress concentrations due to the cooling holes, the "elastic" stress values given in Table VI are seen to be high. In cases of this kind, during the first loading localized plastic deformation occurs, and subsequent changes in pressure differential give rise to conventional fatigue type behavior. Here the actual strain change is small so that the number of cycles to failure is very large. The immediate consequence is deformation rather than failure through cracking. Thus, it appears that the 22 000 gpm coolant flow rate at a

low pool level is tolerable if the implications are fully realized. In any event, the 38 psig average hydrostatic test pressure of the lattice section should not be exceeded. Calculations have shown that the pressure induced moments in the pool side facility flat plate are greater for the hydrostatic test pressure than for the low pool - 22 000 gpm coolant flow rate condition.

The maximum calculated stress in the core box sections encompassed by the obrounds was -10 900 psi. This value takes into account the stress concentration factor of the cooling holes, and is for a coolant flow rate of 22 000 gpm. Although this value is above the code allowable stress for the material, it is below the yield point so there should be no deleterious effects.

In conclusion, it should be stated that in no case should any region of the reactor components be subjected to pressures exceeding the hydrostatic test pressure. The design pressures and hydrostatic test pressures for various regions are given in Table VII.

Table VII. Hydrostatic Test and Design Pressures for Various ORR Regions[a]

Location	Design Pressure (psi)	Hydrostatic Test Pressure (psi)
Obround Section	30	35
Upper Tank Section	40	60
Tank Lattice Section	28[b]	38
Tank D_2O Compartment		20
Beam Hole Tubes	30	45
Lower Tank Section		38
Inlet Water Lines	60	60

[a]Data taken from ORNL Drawing C-24645.

[b]Average pressure between top and bottom of core box.

REFERENCES

1. Expansion Stresses and Reactions in Piping Systems, M. W. Kellogg Company, 1941.

2. J. F. Tavernelli and L. F. Coffin, Jr., "A Compilation and Interpretation of Cyclic Strain Fatigue Tests on Metals," 1958 ASM Reprint No. 112.

3. L. F. Coffin, Jr., "A Study of the Effects of Cyclic Thermal Stresses on a Ductile Metal," Trans. ASME 76, 931 (1954).

4. G. Sachs and A. P. Taber, "Relations Governing Low Cycle Fatigue — A Summary of the Pertinent Literature," Syracuse University Research Institute Report No. MET 575-585111.

APPENDIX

MATERIAL PROPERTIES

The strength properties of the aluminum alloys of which the reactor components are constructed were taken from the Alcoa Aluminum Handbook, Aluminum Company of America, 1959. According to the ASME Boiler and Pressure Vessel Code, Section VIII, "Unfired Pressure Vessels," 1956, the strength properties of welded aluminum structures should be those corresponding to the annealed temper (-O temper) of wrought materials. Therefore, for the tank components and beam hole tubes, the maximum strength properties are taken as those of the -O temper. For the cooling water piping, the -H112 temper was assumed because it corresponds to the lowest strength properties of the 5154 alloy. Table A.I gives the strength properties for each of the materials under consideration.

Table A.I. Material Properties of Aluminum Alloys Used in ORR

Component	Alloy	Ultimate Strength (psi)	Yield Strength (psi)	Endurance Limit[a] (psi)
Cooling Water Return Piping	5154-H112[b]	30 000	11 000	
Lines 137 and 138	6063-T6[b]	30 000	25 000	
Tank Components	5052-O	28 000	13 000	16 000
Dished Head	5154-O	35 000	17 000	17 000
Beam Hole Tubes	1100-O	13 000	5 000	5 000

[a]Based on 500 000 000 cycles of completely reversed stress.

[b]Properties are for pipe only.

The maximum allowable stresses for nonferrous unfired pressure vessels are given in the Unfired Pressure Vessel Code as the lower of the following:

1) One-fourth of the tensile strength as adjusted to minimum, or

2) Two-thirds of the yield strength as adjusted to minimum.

Table A.II gives the code allowable stresses for each of the alloys used in the reactor components under consideration. It should be noted that the utlimate and yield strengths used to obtain these numbers were average values. Therefore, the allowable stresses are slightly high.

Table A.II. Maximum Code Allowable Stresses

Alloy	Maximum Allowable Stress (psi)
5154-H112	7300
6063-T6	7500
5052-0	6250[a]
5154-0	8750
1100-0	2750

[a]This value is given in Table UNF-23 of the 1956 edition of the Unfired Pressure Vessel Code.

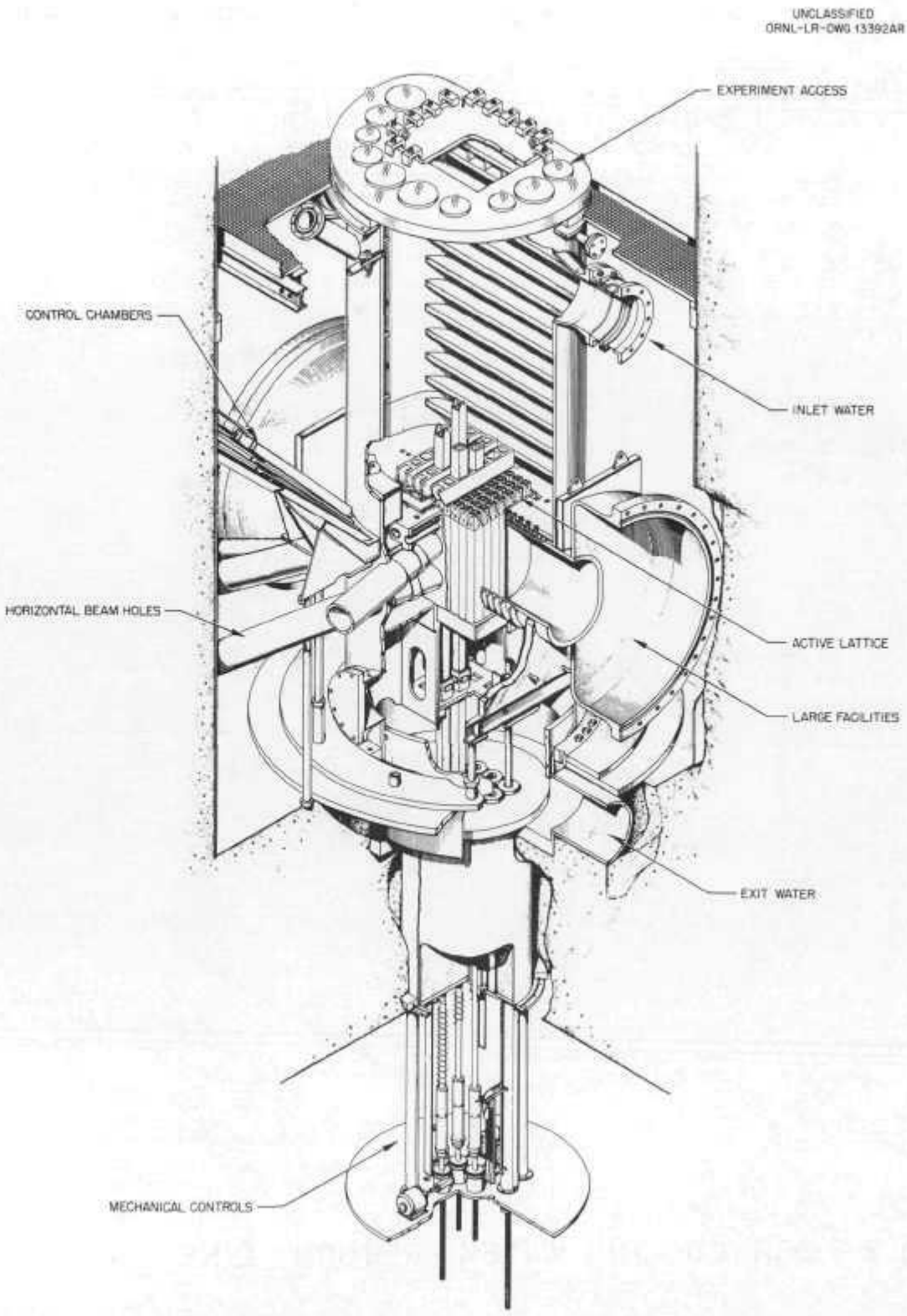

FIG. 1. ORR REACTOR UNIT.

UNCLASSIFIED
ORNL-LR-DWG 49237

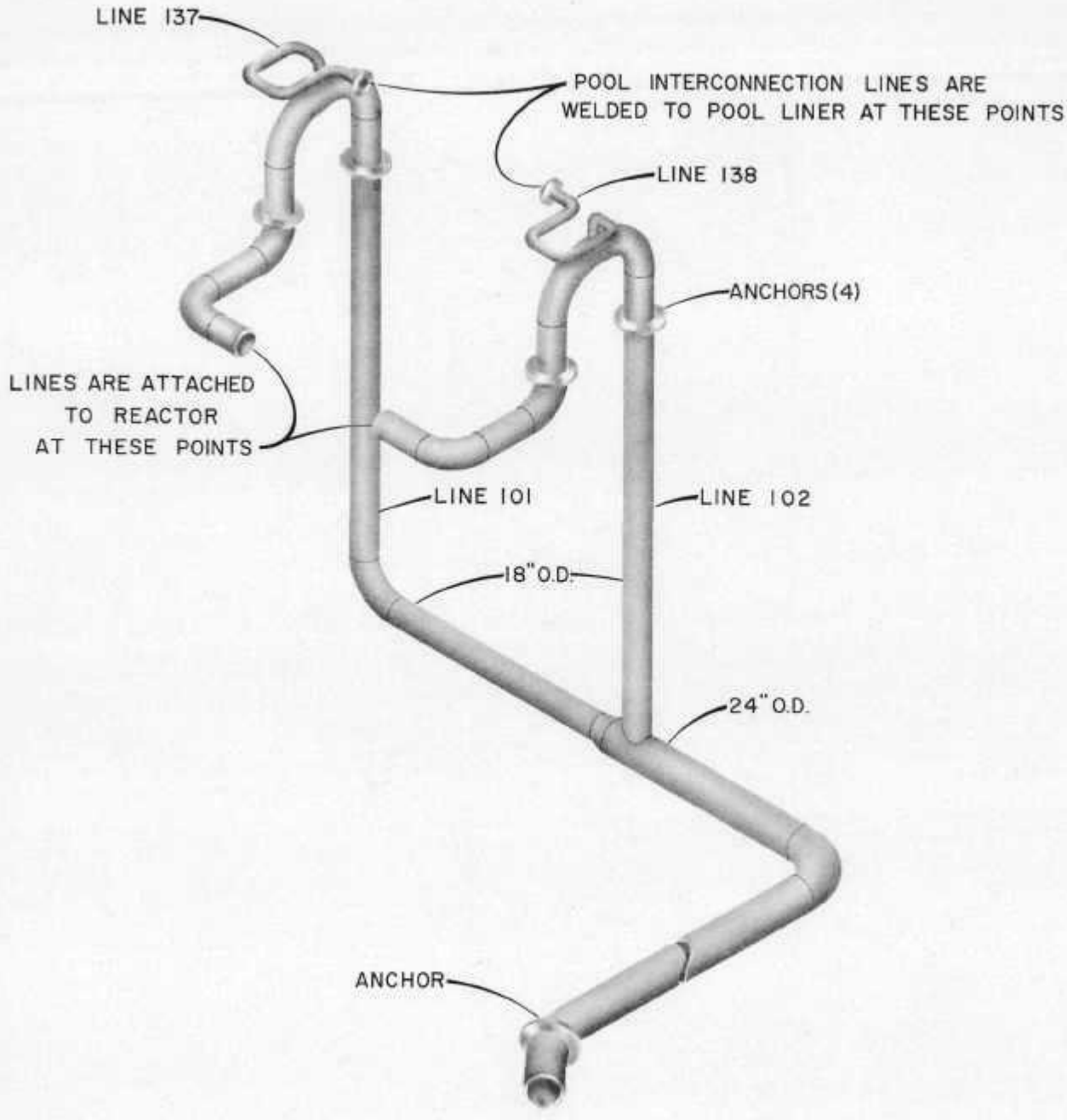

Fig. 2 - ORR COOLING WATER RETURN LINE

UNCLASSIFIED
ORNL-LR-DWG 49235

NOTE: ALL DIMENSIONS IN FEET

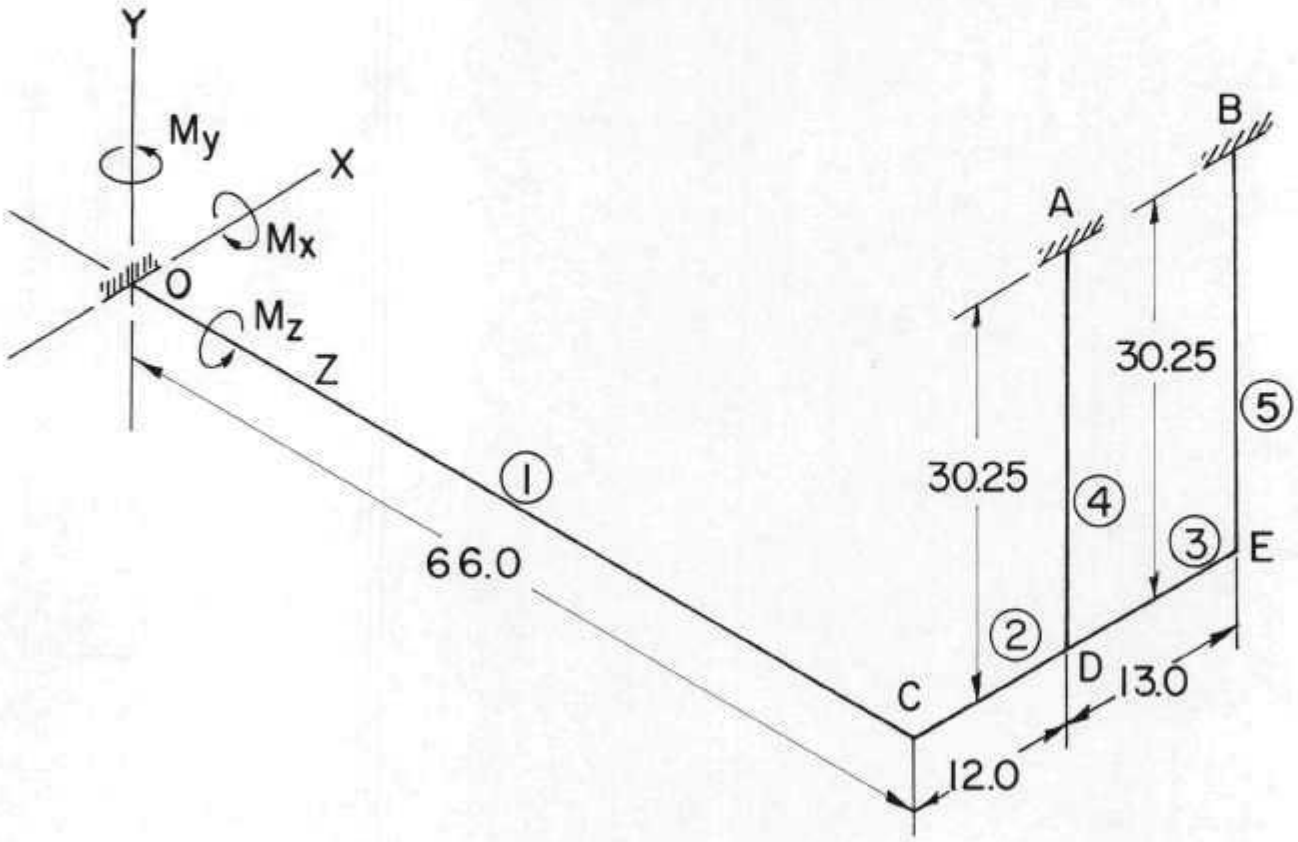

Fig. 3 - PIPE LAYOUT FOR STRESS ANALYSIS
ORR COOLING WATER RETURN LINES 101 AND 102

UNCLASSIFIED
ORNL-LR-DWG 49236

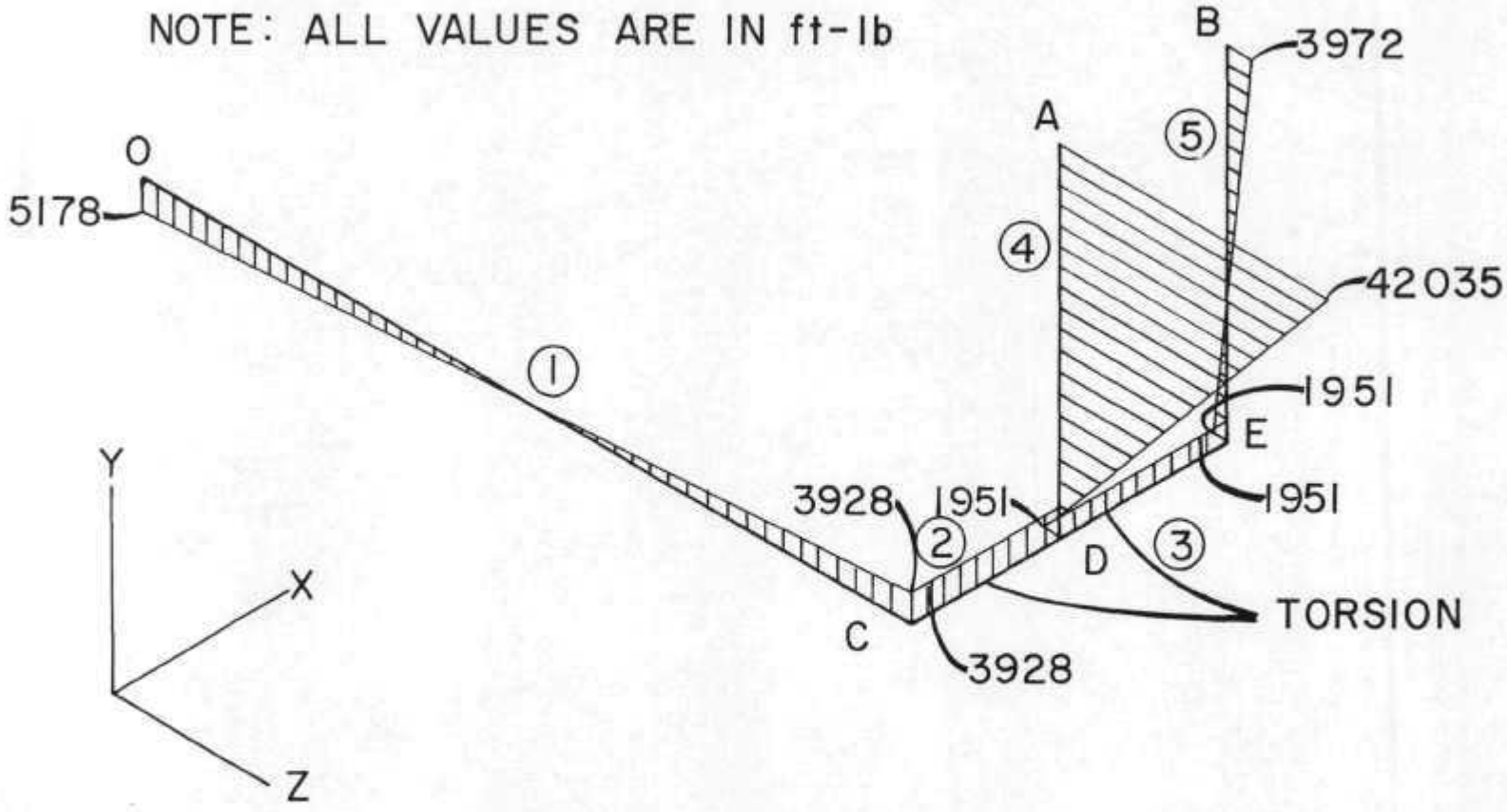

Fig. 4 - MOMENTS IN X PLANE - ORR COOLING WATER RETURN LINES 101 AND 102

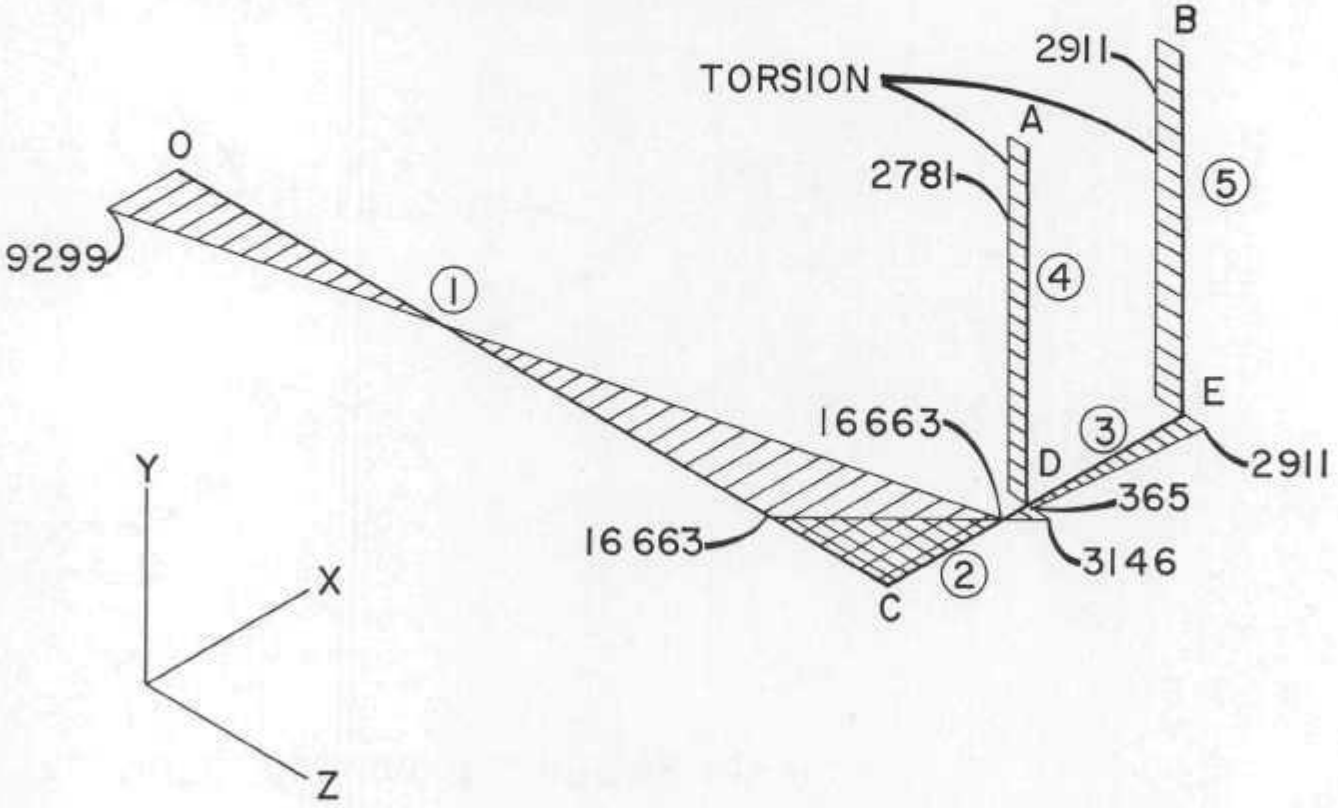

Fig. 5 – MOMENTS IN Y PLANE – ORR COOLING WATER RETURN LINES 101 AND 102

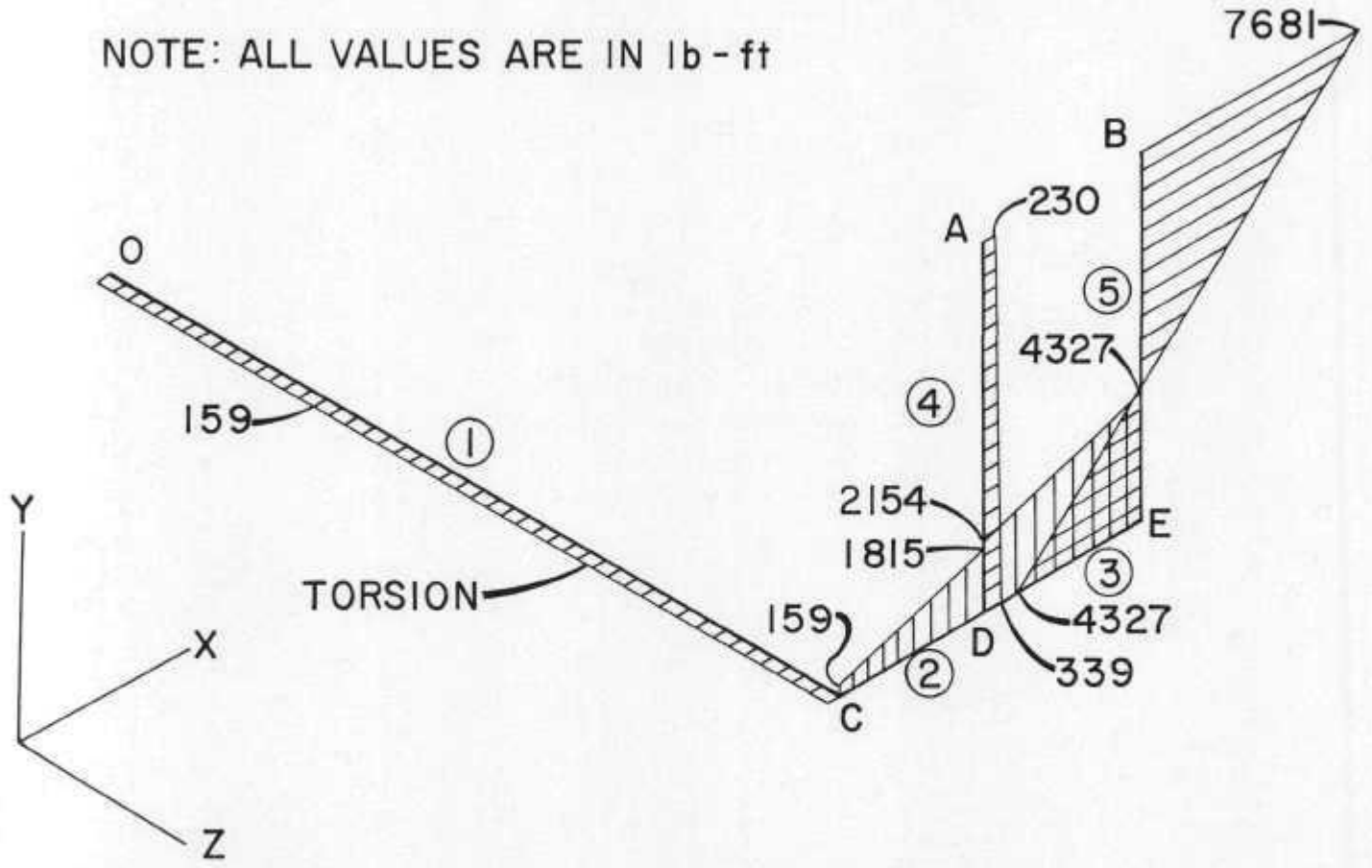

Fig. 6 - MOMENTS IN Z PLANE - ORR COOLING WATER RETURN LINES 101 AND 102

UNCLASSIFIED
ORNL-LR-DWG 49225

NOTE: ALL DIMENSIONS IN FEET

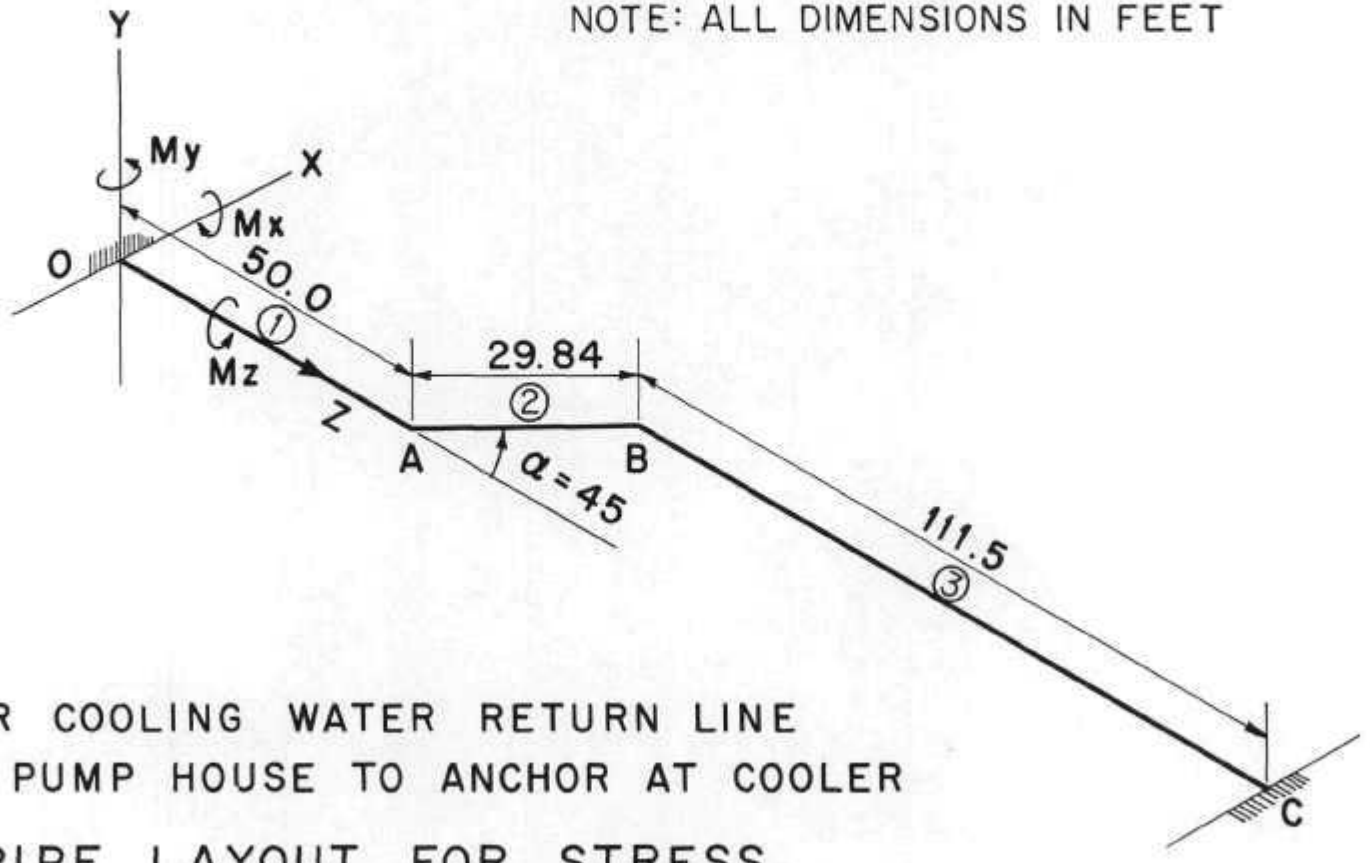

ORR COOLING WATER RETURN LINE
FROM PUMP HOUSE TO ANCHOR AT COOLER

Fig. 7 PIPE LAYOUT FOR STRESS ANALYSIS

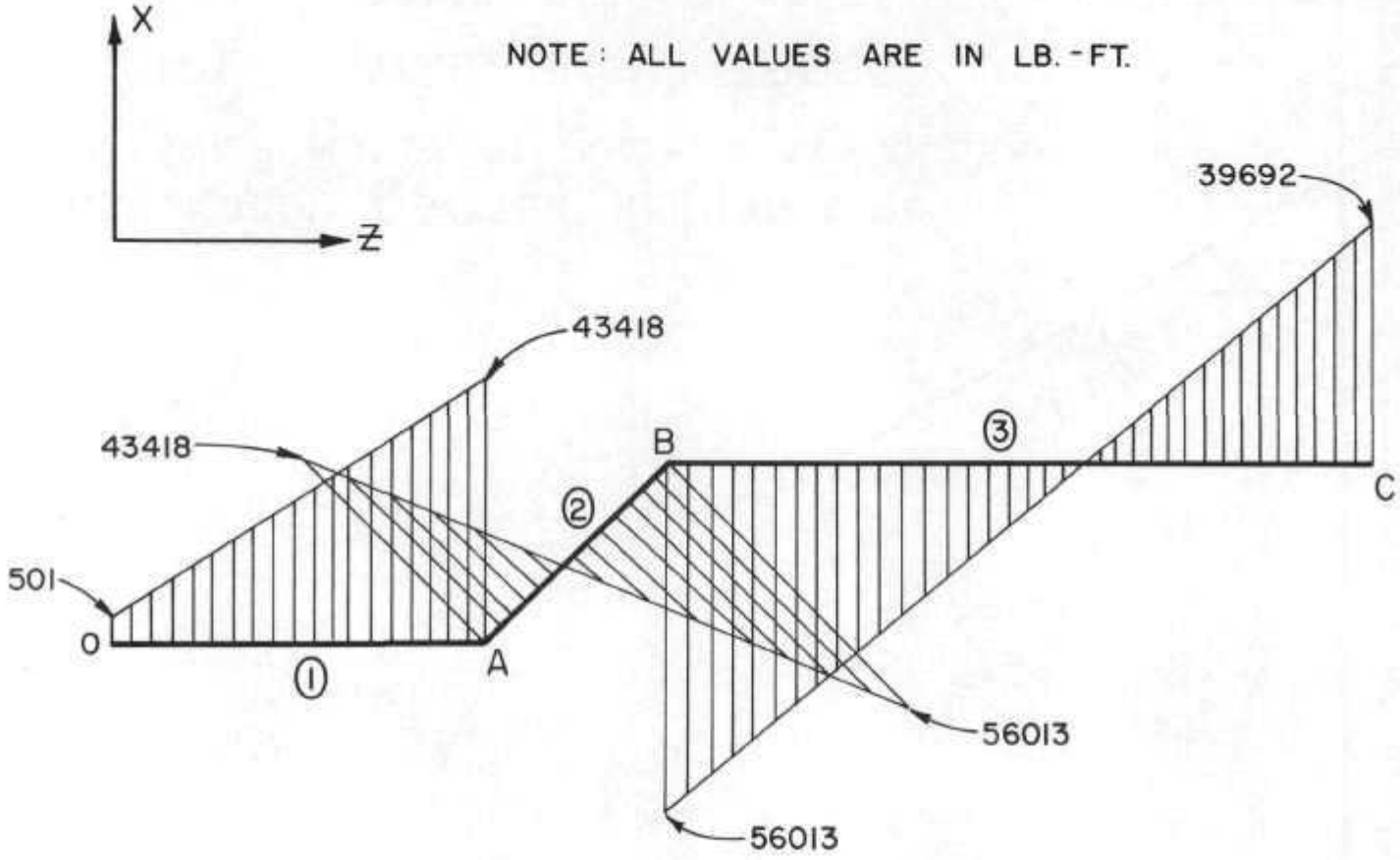

FIG. 8. ORR COOLING WATER RETURN LINE FROM PUMP HOUSE TO ANCHOR AT COOLER

MOMENTS IN Y PLANE

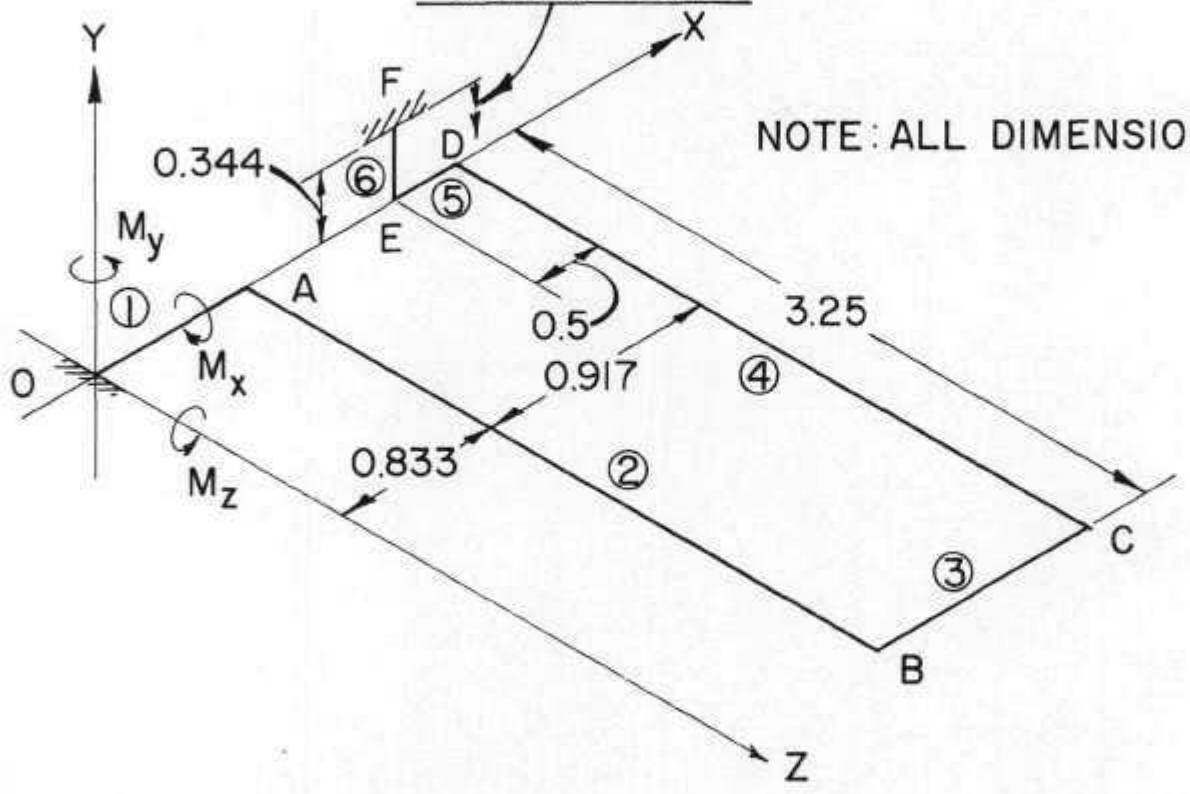

NOTE: ALL DIMENSIONS IN FEET

Fig. 9 - ORR POOL INTERCONNECTION LINES 137 AND 138 PIPE LAYOUT FOR STRESS ANALYSIS

UNCLASSIFIED
ORNL-LR-DWG 49230

NOTE: ALL VALUES IN ft-lb

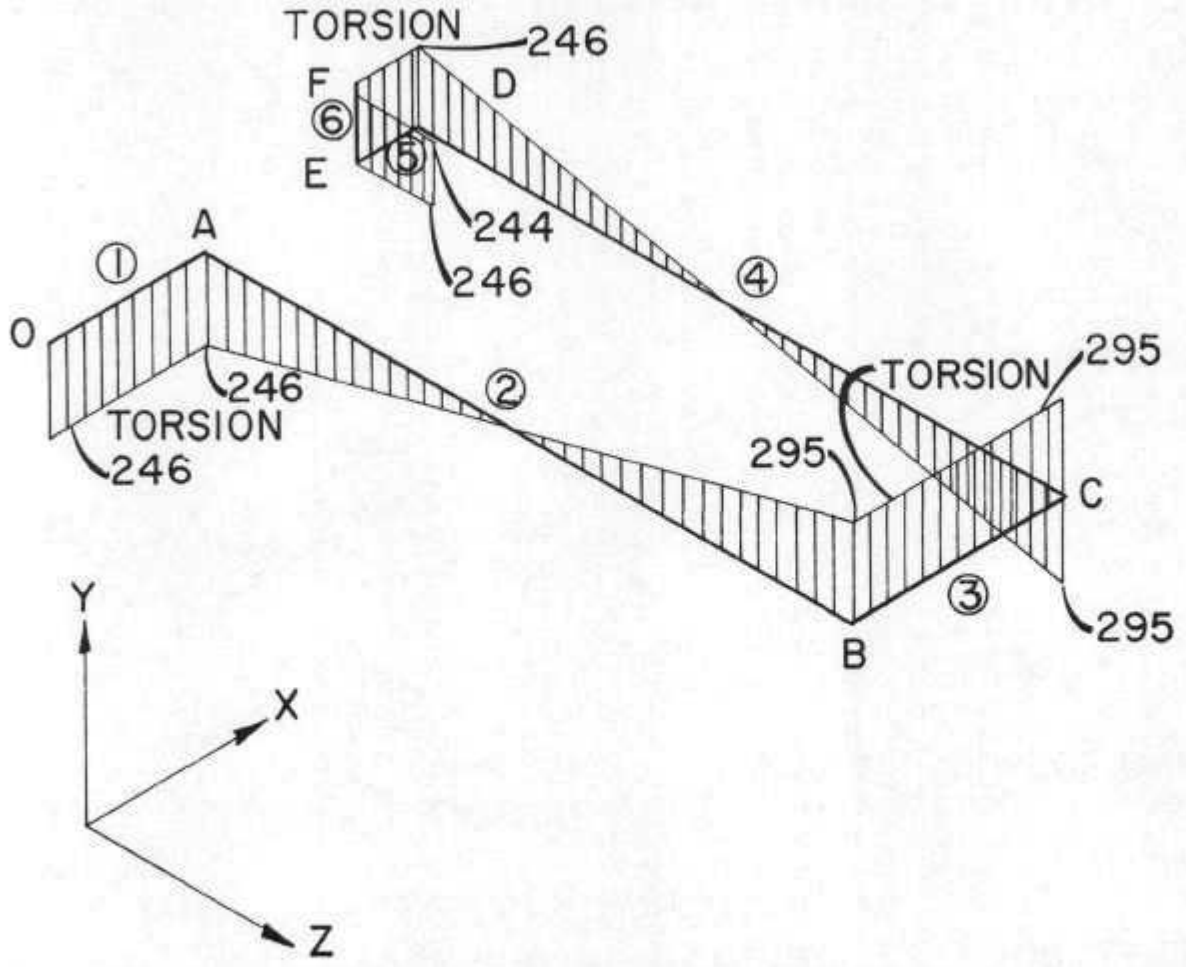

Fig. 10– ORR POOL INTERCONNECTION LINES 137 AND 138 MOMENTS IN X PLANE

UNCLASSIFIED
ORNL-LR-DWG 49229

NOTE: ALL VALUES ARE IN ft-lb

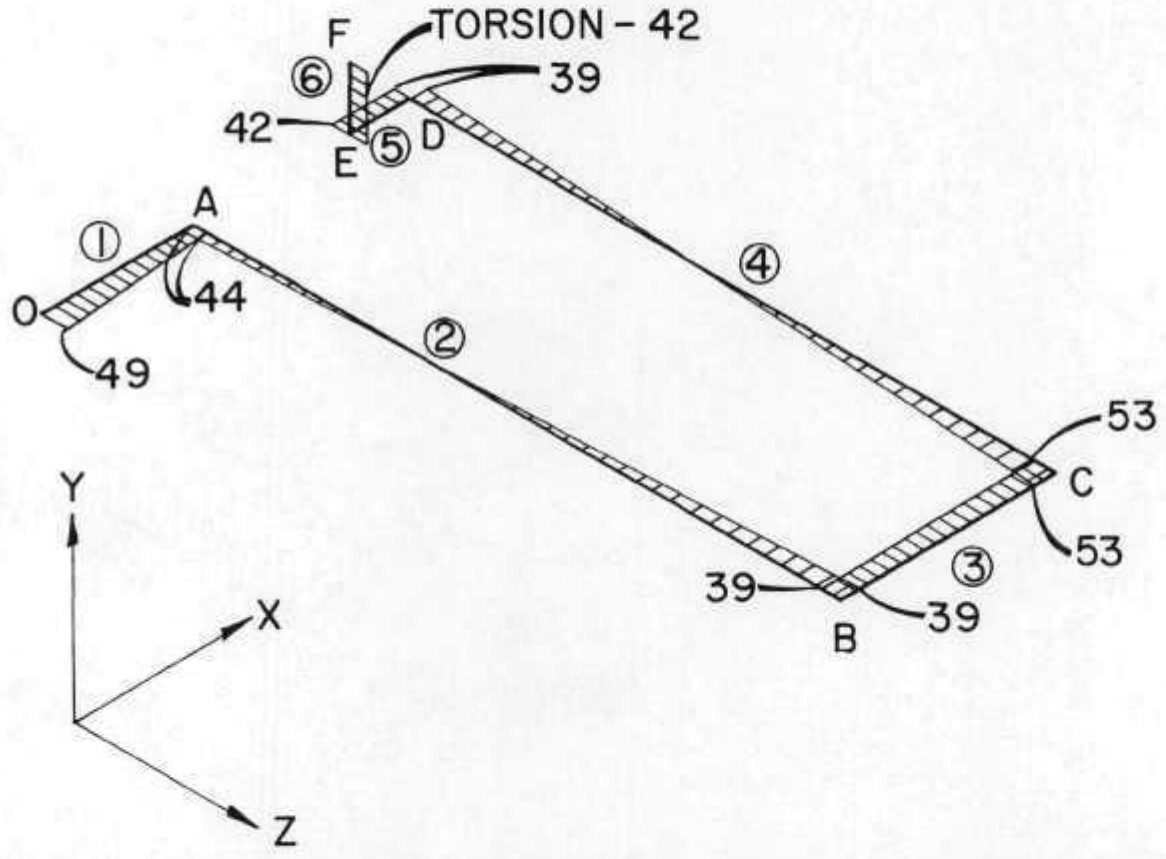

Fig. 11 - ORR POOL INTERCONNECTION LINES 137 AND 138
MOMENTS IN Y PLANE

NOTE: ALL VALUES ARE IN ft-lb

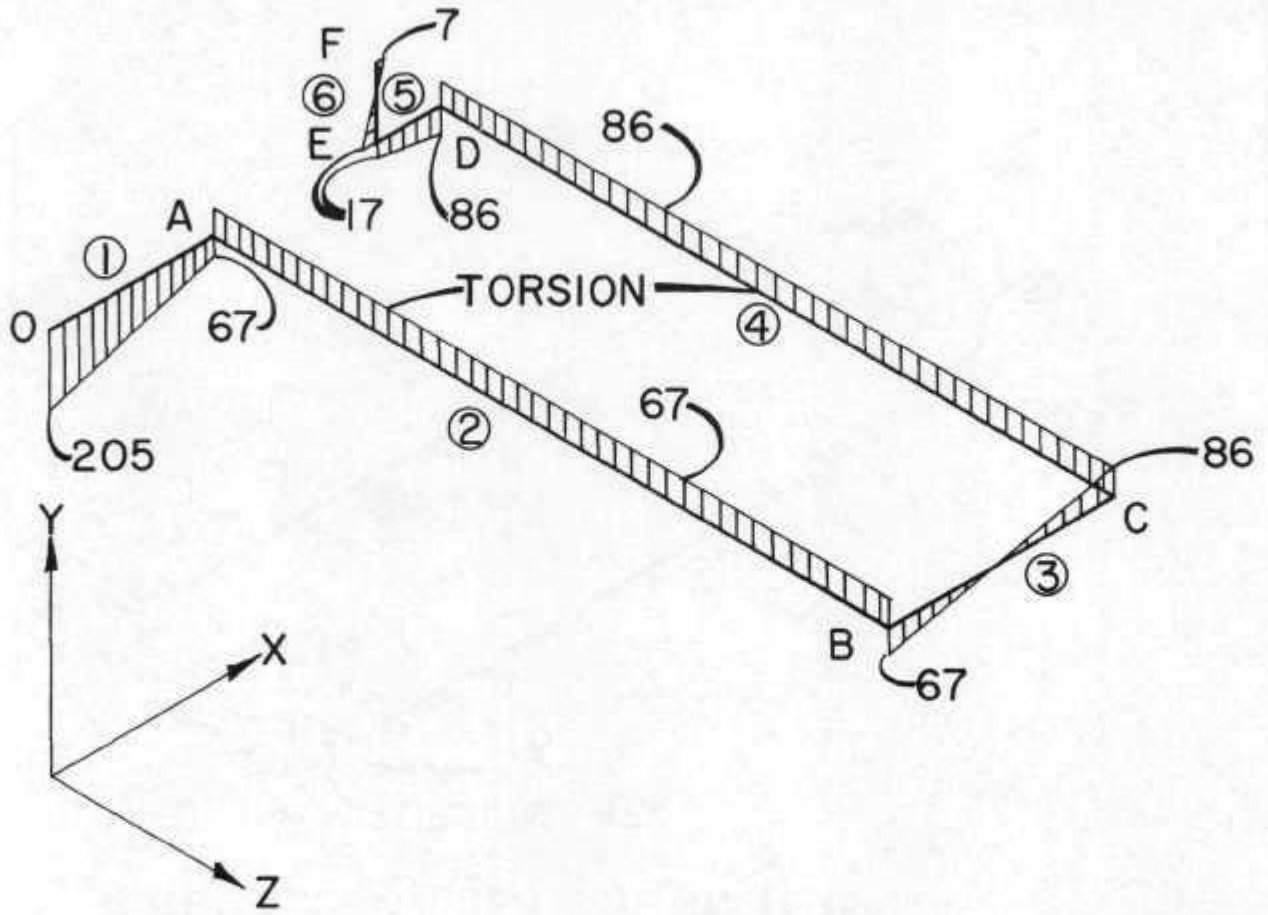

Fig. 12 - ORR POOL INTERCONNECTION LINES 137 AND 138
MOMENTS IN Z PLANE

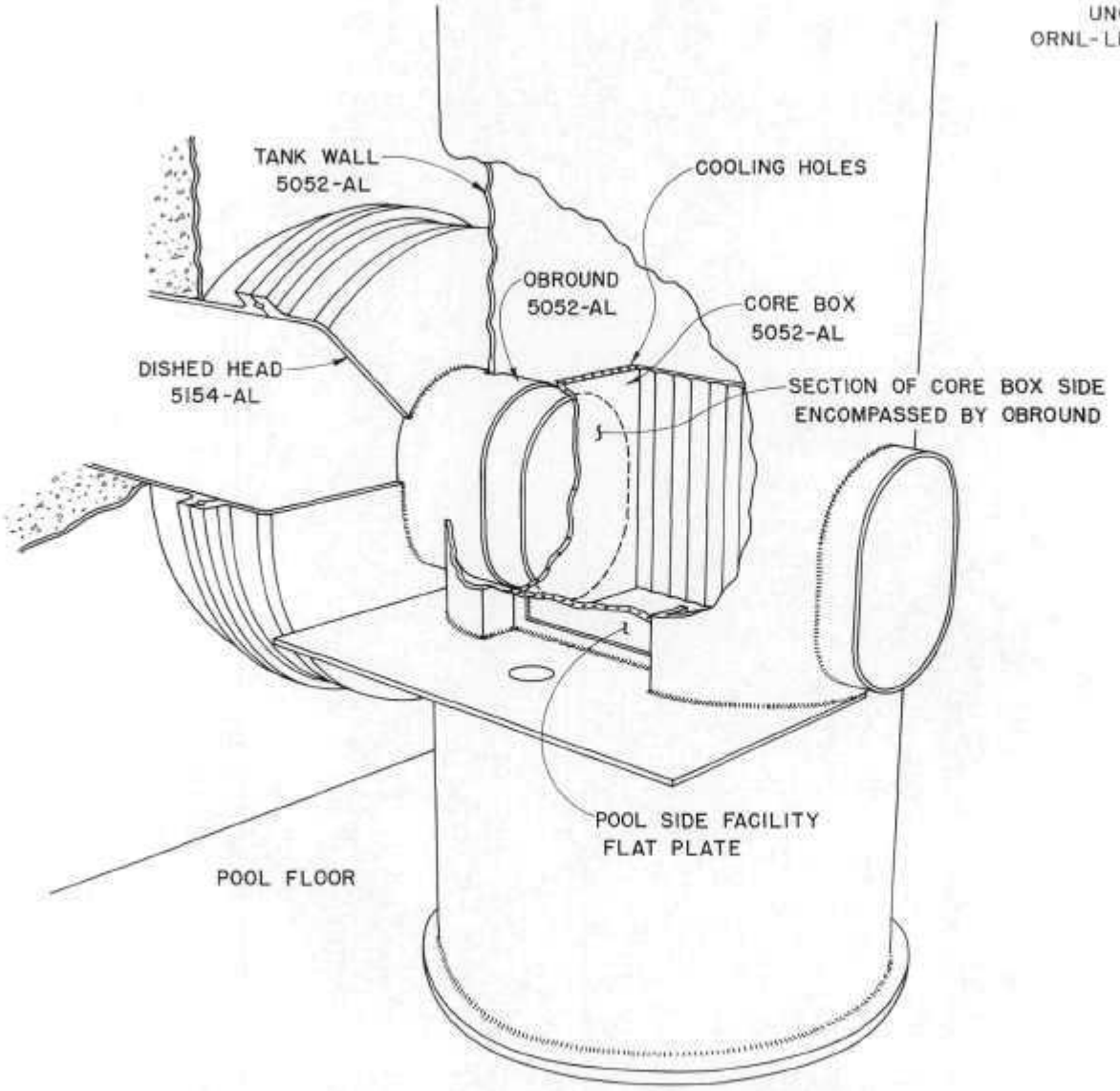

FIG. 13 ORR LARGE FACILITIES

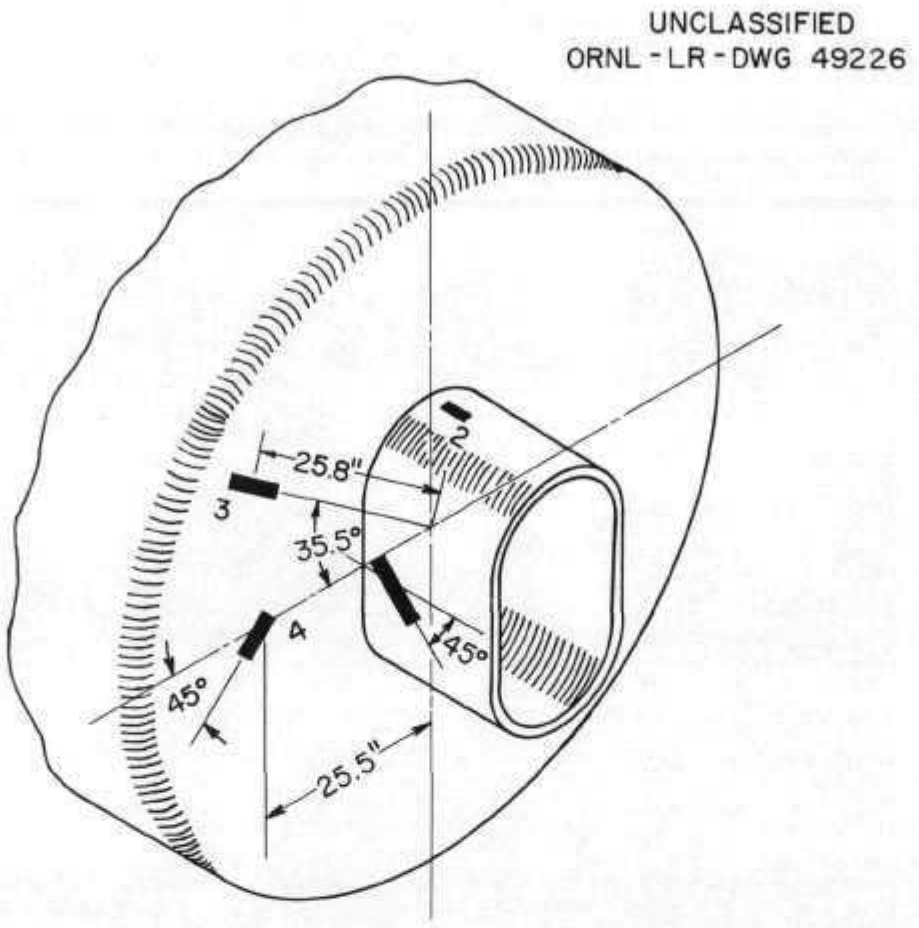

FIG. 14. POSITION OF STRAIN GAGES ON LARGE FACILITY

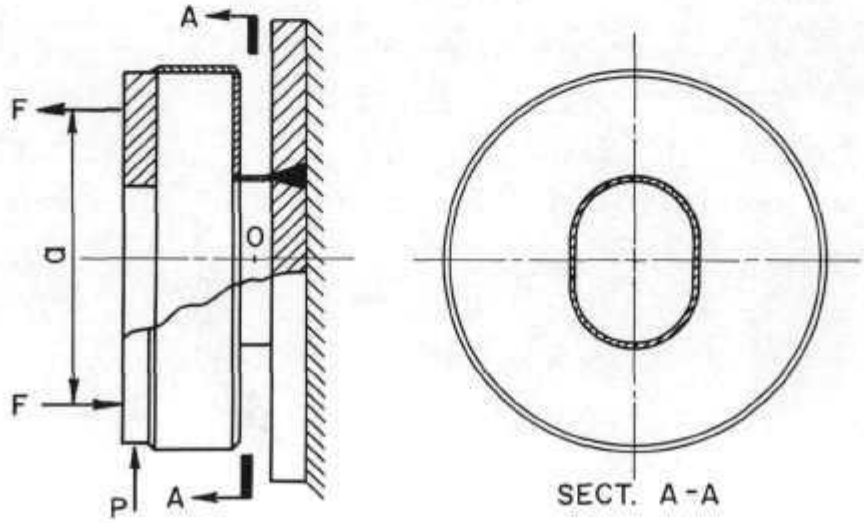

FIG. 15. SCALE MODEL OF LARGE FACILITIES

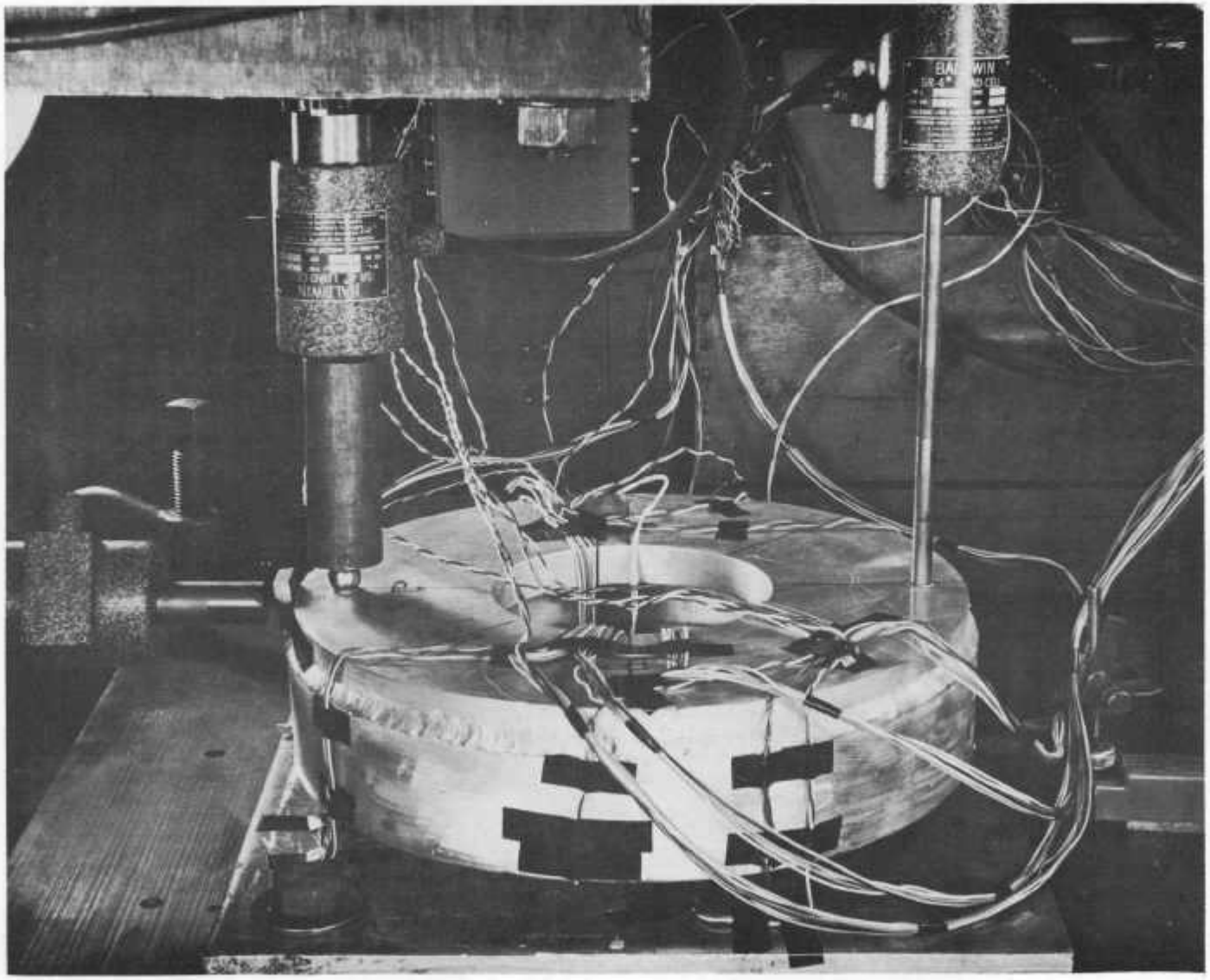

FIG. 16. LARGE FACILITY MODEL DURING TESTING.

UNCLASSIFIED
ORNL - LR - DWG 49231

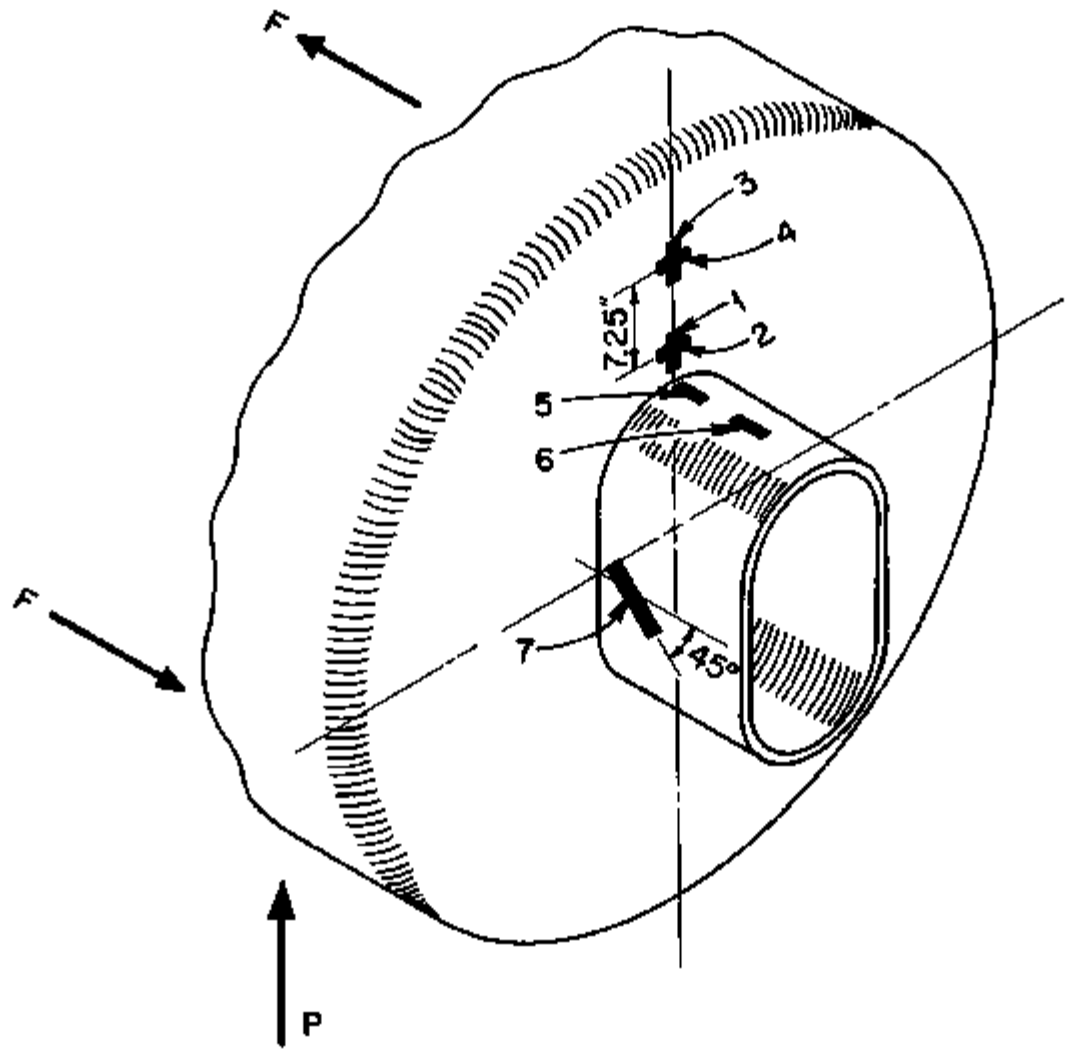

FIG. 17. SEVEN KEY STRAIN GAGE POSITIONS ON LARGE FACILITY MODEL

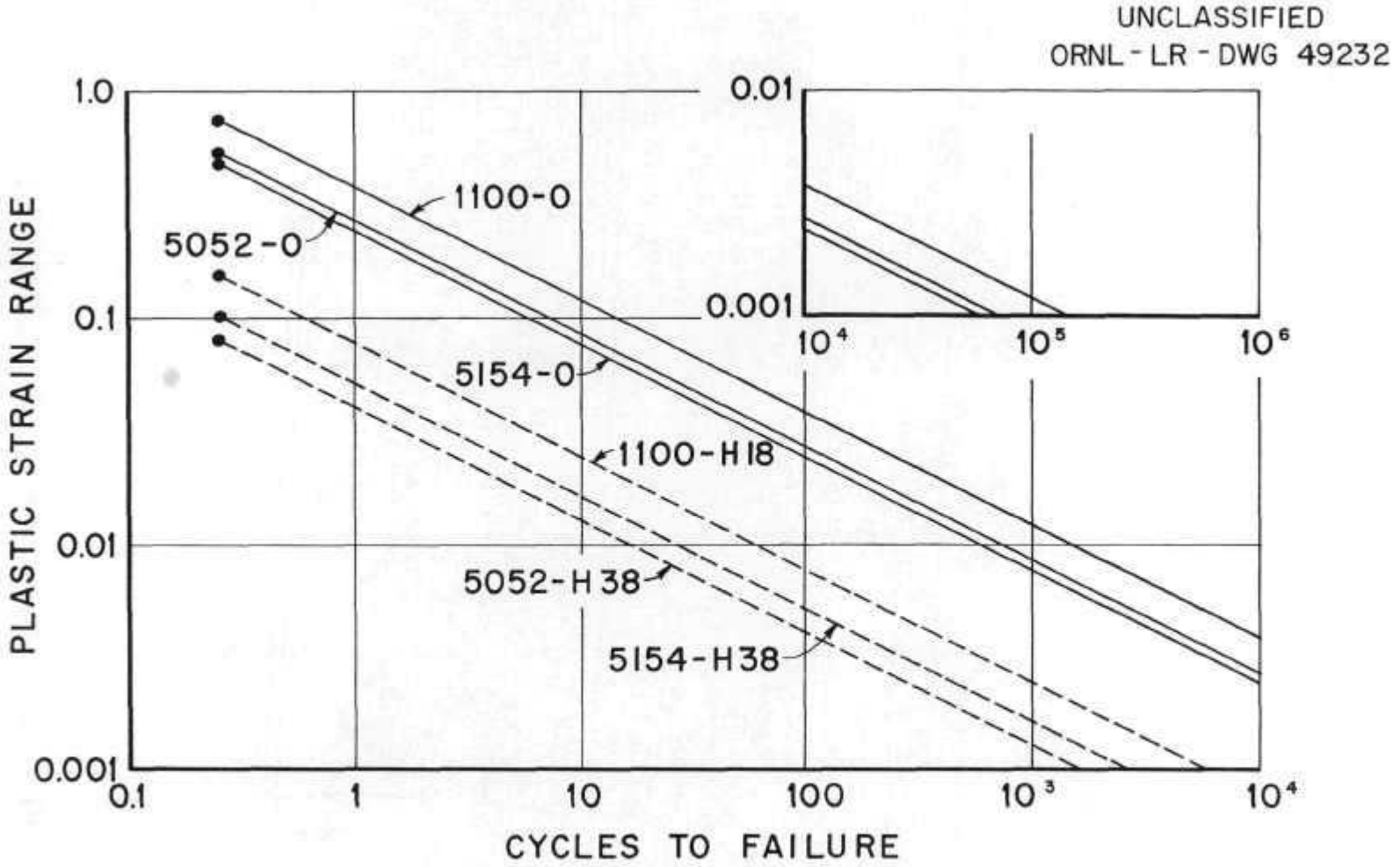

Fig. 18 PLASTIC STRAIN RANGE
VERSUS
CYCLES TO FAILURE
FOR 1100-0, 5052-0, & 5154-0 Al

UNCLASSIFIED
ORNL - LR - DWG 49224

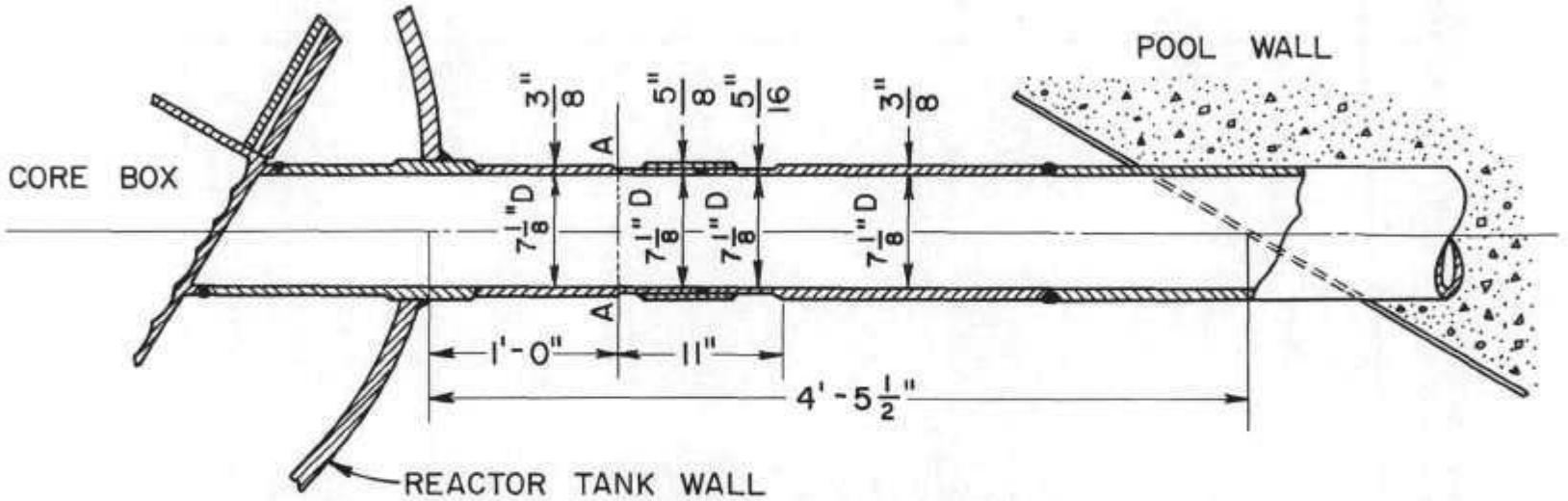

FIG. 19. BEAM HOLE TUBE B-6
MATERIAL - 1100 Al

UNCLASSIFIED
ORNL - LR - DWG 49223

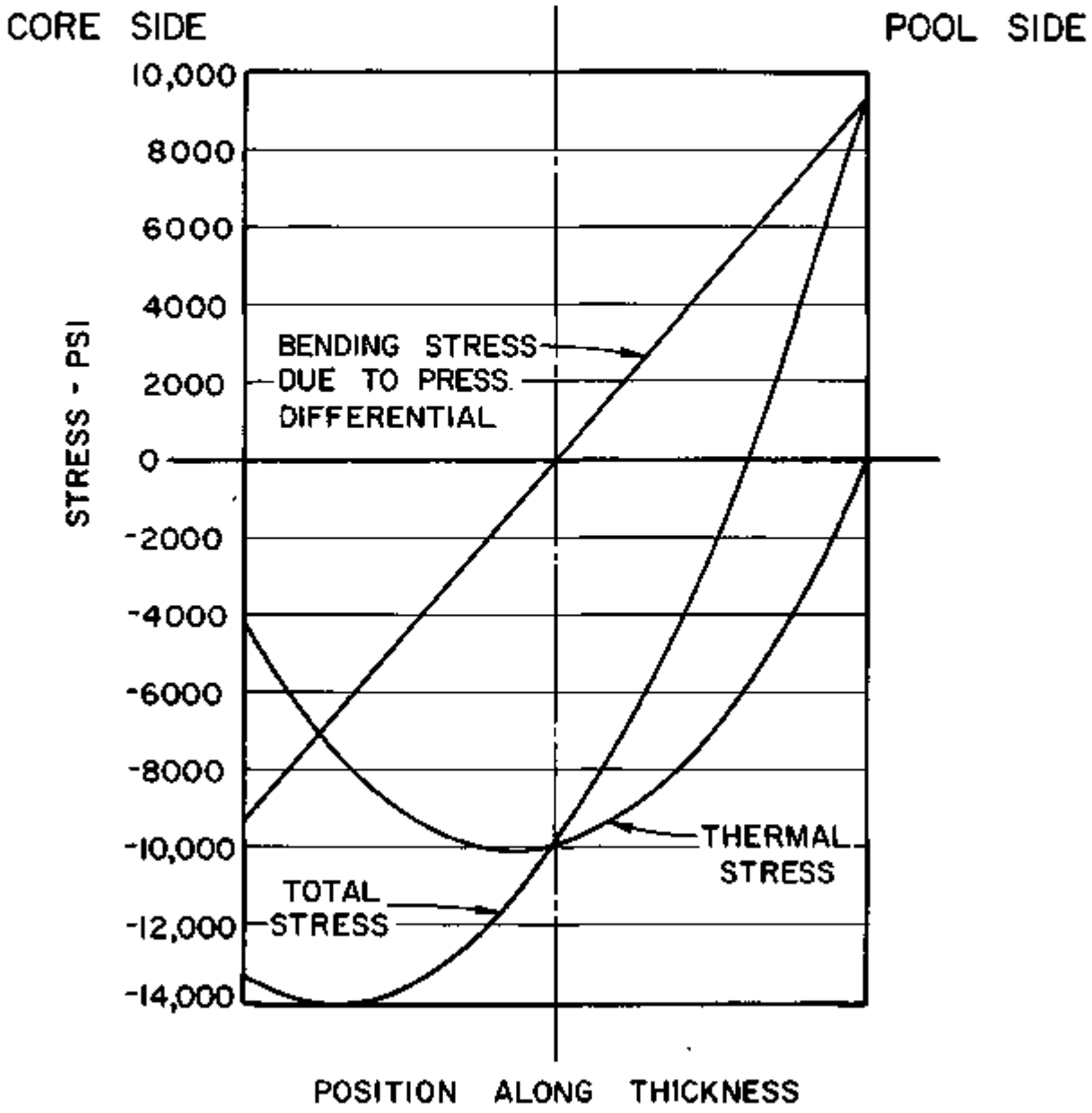

FIG. 20. STRESS IN ORR POOL SIDE FLAT PLATE
LOW POOL LEVEL - 22,000 gpm COOLANT FLOW RATE

DISTRIBUTION

Internal

1. M. Bender
2. F. T. Binford
3. A. L. Boch
4. E. J. Breeding
5. C. D. Cagle
6. W. R. Casto
7. R. H. Chapman
8. R. A. Charpie
9. R. D. Cheverton
10. T. E. Cole
11-13. J. M. Corum
14. B. Y. Cotton
15. W. B. Cottrell
16. J. A. Cox
17. G. A. Cristy
18. D. A. Douglas
19. J. Foster
20. A. P. Fraas
21. D. R. Gilfillan
22. J. P. Gill
23-26. B. L. Greenstreet
27. H. Grimac
28. P. R. Kasten
29. B. W. Kinyon
30. H. G. MacPherson
31. R. V. McCord
32. W. D. Manly
33. J T. Meador
34. E. C. Miller
35. S. E. Moore
36. A. M. Perry
37. C. A. Preskitt
38. M. E. Ramsey
39. G. C. Robinson
40. M. W. Rosenthal
41. A. F. Rupp
42. G. Samuels
43. W. L. Scott
44. M. J. Skinner
45. F. J. Stanek
46. W. H. Tabor
47. J. R. Tallackson
48. A. M. Weinberg
49. J. F. Wett, Jr.
50. C. E. Winters
51. F. J. Witt
52. Laboratory Records - RC
53-62. Laboratory Records
63-64. Central Research Library
65. Document Reference Section
ORNL-Y-12 Technical Library
66-80. TISE

External

81. C. Fisher, University of Tennessee
82. R. W. Holland, University of Tennessee
83. R. L. Maxwell, University of Tennessee
84. M. Milligan, University of Tennessee
85. L. R. Shobe, University of Tennessee
86. C. Wilson, University of Tennessee